


NANO EXPRESS

Open Access



Boosting Power Conversion Efficiency of Quantum Dot-Sensitized Solar Cells by Integrating Concentrating Photovoltaic Concept with Double Photoanodes

Pei Xu¹, Xiaopeng Chang¹, Runru Liu^{1*}, Liying Wang², Xuesong Li², Xueyu Zhang², Xijia Yang², Dejun Wang¹ and Wei Lü^{2*} 

Abstract

Despite great efforts dedicated to enhance power conversion efficiency (PCE) of quantum dot-sensitized solar cells (QDSSCs) in the past two decades, the efficiency of QDSSCs is still far behind its theoretical value. The present approaches for improving PCE are mainly focused on tailoring the bandgap of QDs to broadening light-harvesting and optimizing interfaces of component parts. Herein, a new solar cell architecture is proposed by integrating concentrating solar cell (CPV) concept into QDSSCs with double photoanode design. The Cu₂S mesh is used as a counter electrode and sandwiched between two photoanodes. This designed battery structure can increase the PCE by 260% compared with a single photoanode. With the most extensively used CdS/CdSe QD sensitizers, a champion PCE of 8.28% ($V_{oc} = 0.629$ V, $J_{sc} = 32.247$ mA cm⁻²) was achieved. This is mainly due to the increase in J_{sc} due to the double photoanode design and adoption of the CPV concept. In addition, another reason is that concentrated sunshine illumination induced a photothermal effect, accelerating the preceding chemical reactions associated with the conversion of polysulfide species. The cell fabrication and design reported here provides a new insight for further development of QDSSCs.

Keywords: Quantum dot-sensitized solar cells, Concentrating photovoltaic, Double photoanodes, Mesh counter electrode

Introduction

As a kind of promising and comparably economic photoelectrical conversion device, quantum dot-sensitized solar cells (QDSSCs) have attracted great attention due to their high theoretical power conversion efficiency (PCE) [1, 2]. QDSSCs inherit the structure of dye-sensitized solar cells, including photoanode (typically, a layer of porous oxide semiconductor with a wide bandgap covered by

semiconductor QDs as sensitizers), liquid electrolyte, and counter electrode. In order to enhance cell PCE for potential commercial application, numerous strategies have been investigated mainly from material viewpoints, involving synthesizing new QD sensitizers for broadening light-harvesting range; preparing photoanodes with different nanostructures such as porous film [3], nanotube [4, 5], and nanorod for better electron extracting [6, 7]; fabricating noble metal-doped photoanode using localized surface plasmon resonance [8, 9]; developing sulfide and other counters to replace Pt counter; synthesizing different electrolytes; and so on.

One of the most important factors limiting the photoelectric conversion efficiency of QDSSCs is the narrow

* Correspondence: runruli@sina.com; lw771119@hotmail.com

¹Key Laboratory of Materials Design and Quantum Simulation, College of Science, Changchun University, Changchun 130012, People's Republic of China

²Key Laboratory of Advanced Structural Materials, Ministry of Education & Advanced Institute of Materials Science, Changchun University of Technology, Changchun 130012, People's Republic of China

absorbing range of solar radiation [10]. The absorption region is strongly dependent upon photoanode thin film and QDs. Narrowing bandgap of QDs is an effective way for broadening light-harvesting range. Zhong et al. synthesized Zn–Cu–In–Sn alloyed QDs and greatly improved the PCE of QDSSCs, setting several PCE records of QDSSCs [11–13]. Currently, the reported highest PCE of QDSSCs is 14.02% achieved by Zhao et al. [14]. In their work, Zn–Cu–In–Sn alloyed QDs were used as a sensitizer, and the counter electrode (CE) is CuS doped with carbon nanotubes and graphene, which initiated a new level of the PCE of QDSSCs. However, excessively decreasing the bandgap to enhance sunlight harvesting will induce the open-circuit voltage loss and decrease the device performance due to the downshift of the conduction band edge.

To further improve cell performance, device configuration has been taken into account. In dye-sensitized solar cells and colloidal quantum dot solar cells [15], tandem structures have already been used as a significant approach to break through the PCE limitations [16, 17]. For most tandem structures of dye-sensitized solar cells, a semi-transparent Pt on conductive glass or Pt mesh is applied in the middle of the cell as the counter electrode [18]. TiO_2 films are separated into two or more layers sensitized by the same or different dyes, which can broaden the spectral response and thereby significantly improve the cell performance [19–21]. For QDSSCs, Meng et al. design a double photoanode structure with a semi-transparent mesh-structured Cu_2S counter electrode sandwiched between two TiO_2 photoelectrodes. Under the one sun illumination from the top electrode, the optimized cell shows a 12% increase in PCE [22]. In their work, the tandem structure was used in QDSSCs for the first time. However, the light utilization efficiency of the battery tandem structure is limited. Xu et al. demonstrated the NIR light-enhanced polysulfide reduction at the electrode–electrolyte interface by illuminating the CuS counter electrode with NIR light, showing a 15% increase in PCE, which is attributed to photothermal effect and plasmonic resonance absorption [23].

Thanks to the great efforts in the past several decades, the PCE of QDSSCs is allowed to be comparative with that of the parallel device, dye-sensitized solar cell. However, the efficiency of QDSSCs is still far behind its theoretical value, and it still remains to be solved for commercial application. Therefore, exploring new strategy to boost PCE of QDSSCs is still an urgent task. Herein, we integrate concentrating photovoltaic concept into QDSSCs with double porous TiO_2 photoanodes and Cu_2S mesh counter electrode design [24], achieving a 260% increase in PCE compared with the traditional single photoanode device. With the most extensively used CdS/CdSe QD sensitizers, a champion PCE of 8.28% ($V_{\text{oc}} = 0.629 \text{ V}$, $J_{\text{sc}} = 32.247 \text{ mA cm}^{-2}$) is achieved.

Light management as an important technology to improve the conversion efficiency in solar cells aims to increase the photon flux received by solar cells [25]. The light-trapping structure is a commonly used method for light management, including mirrors [26, 27], Lambertian surfaces [28], and textured surfaces [29, 30]. By the light-trapping effect, the optical path length is increased, thereby improving the PCE of solar cells. One of the basic light-trapping structures is to prepare a mirror on the back surface of the solar cell, and the reflectivity of the mirror can be as high as 95% [31]. Inspired by the above discussion, Fig. 1 illustrates the device architecture used in the present work. Double TiO_2 photoanode design is adopted, which is separated by Cu_2S mesh as the counter electrode. The thickness of the TiO_2 photoanode is about $4.5 \mu\text{m}$, which can be seen in Fig. S1. The top cell and the bottom cell use the same material and structure, so it is not necessary to consider the lattice constant and expansion coefficient of different semiconductor materials in the two photoanodes. The Cu_2S grown on Cu mesh as the counter electrode allows the transmitted light from the top cell to arrive bottom photoanode. The wide bandgap materials at the top filter out high energy photons, and the low energy photons pass through them and then absorbed by the narrow bandgap materials at the bottom cell. Apparently, the PCE of the double photoanode structure is higher than that of the single photoanode structure because the double photoanode structure can capture more light and thus increase current density. However, illuminating only from the top direction induces just an 18% increase in PCE compared with a single photoanode device as shown later, which is due to the strong absorption and reflection of sunshine by the top cell, leaving inadequate light density for the bottom cell [22].

Considering that the captured light of the bottom cell is limited, we introduce the concept of concentrating photovoltaic cell (CPV) into the current device [32, 33] and set a parabolic reflector under the bottom photoanode. CPV systems use optical elements to focus light on a small area of solar cells, which improves the efficiency of photovoltaic technology while minimizing costs. The reduction of cell area can make the cost of CPV compete with flat panel photovoltaic. As shown in Fig. 1, the parabolic reflector makes focused light on the bottom photoanode. By controlling the distance between the reflector and the bottom photoanode, the active area could be adjusted to match the area of the cell. In addition, the augmented light could transmit and get to the top photoanode, providing additional excitation energy for light harvesting. Of course, the photothermal effect caused by CPV should have an impact on the PV performance [34], which will be discussed in detail later.

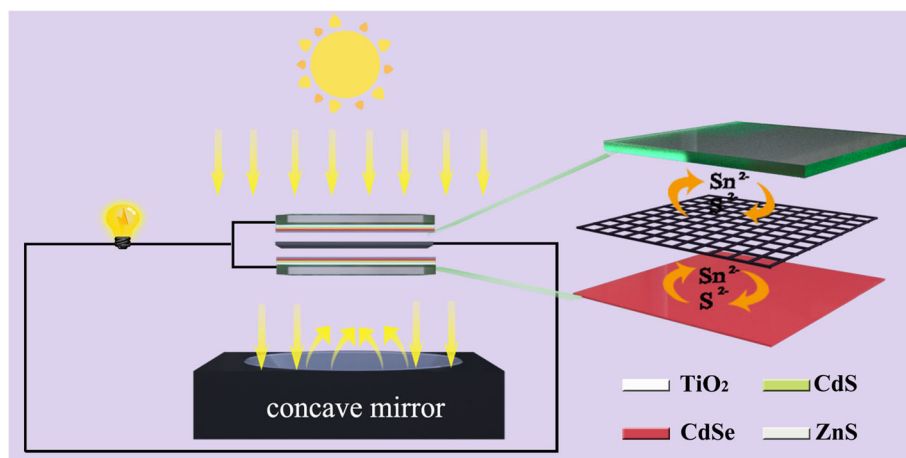


Fig. 1 Schematic diagram of the cell design in the present work

Methods

Materials

Titanium dioxide (99.8%, 10–25 nm, TiO₂) and sodium sulfite (AR, Na₂SO₃) were supplied from Aladdin. Fluorine-doped tin oxide conducting glass (FTO, thickness 1.6 mm, transmittance 83%, sheet resistance 15/square) was purchased from Zhuhai Kaivo Optoelectronic Technology Co., Ltd. (China). Methanol (AR, CH₃OH), ethanol (AR, CH₃CH₂OH), and acetone (AR, CH₃OCH₃) were supplied by Beijing Chemical Works (China). Ethylenediamine (AR, C₂H₈N₄) and selenium (AR, Se) were purchased from Tianjin Guangfu Fine Chemical Research Institute (China). Hydrochloric acid (36%, HCl), ethyl cellulose ethoate (AR, [C₆H₇O₂(OC₂H₅)₃]_n), alpha-terpineol (AR, C₁₀H₈O), cadmium acetate (AR, Cd(CH₃COOH)₂), zinc acetate (AR, Zn(CH₃COOH)₂), sodium sulfide (AR, Na₂S·9H₂O), sulfur (AR, S), and thiourea (AR, CH₄N₂S) were supplied by Sino-pharm Chemical Reagent Co., Ltd. (China). Nitrilotriacetic acid trisodium (98%, C₆H₉NNa₃O₆) was purchased from TCI (Shanghai) Chemical Industry Development Co., Ltd. (China). Brass mesh was supplied by Hebei Xingheng Wire Mesh Products Co., Ltd. (China).

Preparation of the Cu₂S Counter Electrode

The brass mesh was soaked in HCl (36%) for 2 h at 70 °C to remove the zinc on the surface of the Cu mesh. The copper mesh was rinsed with deionized water and dried at room temperature after removing the copper mesh from the solution. Then, the Cu mesh was immersed into an aqueous solution containing 1 M Na₂S and 1 M S for 5 s to get flake Cu₂S, followed by washing with deionized water and drying at room temperature. To prepare granular Cu₂S, the Cu mesh treated with HCl (36%) was immersed in a mixed solution of CH₄N₂S (0.01 M) and C₂H₈N₄ (0.4 ml) for 24 h, followed by washing with deionized water and drying at room temperature.

Preparation of CdS/CdSe QDs Co-sensitized TiO₂ Photoanode

TiO₂ mesoporous film was prepared by spin-coating a paste containing TiO₂ (0.01 M), EC (0.4 g), C₁₀H₈O (3.245 g), and CH₃CH₂OH (8.5 ml) on cleaned FTO substrates, which was dried in an oven at 60 °C and followed by annealing at 450 °C for 30 min to remove the organic solvents. The rotation speed of the spin coater is 7500 rpm for 30 s. The successive ionic layer adsorption and reaction (SILAR) process was employed to deposit the CdS QDs. Typically, the TiO₂ film was alternately dipped into methanol solution of Cd(CH₃COOH)₂ (0.12 M) and Na₂S solution (0.02 M with methanol and deionized water 1:1 v/v) for 30 s in each cycle for total 5 cycles. CdSe QDs were coated by chemical bath deposition (CBD) method. In detail, a solution containing Cd²⁺ and Se²⁻ source was prepared by the following method. 1.55 g Na₂SO₃ was dissolved in 25 ml deionized water. 0.155 g Se powder as Se²⁻ source was added into the above solution. The obtained solution was heated with an oil bath at 125 °C for 3 h under stirring condition. The Cd²⁺ solution was prepared by mixing 25 ml nitrilotriacetic acid deionized water solution (120 mM) and 25 ml Cd(CH₃COO)₂ deionized water solution (80 mM). Then, the prepared Se²⁻ solution and Cd²⁺ solution were mixed together. The as-prepared CdS-coated photoanodes were put into the above mixed solution at 24 °C for 2 h in the dark. For the ZnS passivation, the sensitized films were deposited by dipping into 0.1 M Zn(CH₃COO)₂ and 0.1 M Na₂S (with methanol and water 1:1 v/v) solutions for 1 min alternately and 4 cycles. The active area of the solar cell is 0.25 cm². The polysulfide electrolyte (2 M Na₂S and 2 M S solution with methanol and deionized water 7:3 v/v) was transfused into the cell via injector.

Electrochemical Measurement

Electrochemical analysis was fulfilled by the DyneChem electrochemical workstation, and platinum and Ag/AgCl are used as the counter electrode and reference electrode, respectively. The cyclic voltammogram and tafel polarization curves were tested in 2 M polysulfide electrolyte. Nyquist plots of QDSSCs are under the illumination of one full sun intensity. The voltage used during the EIS measurements is 0.5 V.

Characterization

The surface morphology was analyzed by scanning electron microscopy (SEM) (JEOL7610), the characterization of samples was measured by X-ray photoelectron spectroscopy (XPS) (Kratos Axis UltraDLD), and the J - V curves of QDSSCs were measured by Keithley 2400 source meter (Zolix Instruments Co., Ltd.). IR temperature images are obtained by FLIR T460.

Results and Discussion

There are numerous nanostructured materials that can be used as counter electrodes for QDSSCs, including

Cu_2S , CoS , GeC [35], and NCW [36]. However, the Cu_2S counter electrode based on brass mesh exhibits ideal catalytic activity toward $\text{Sn}^{2+}/\text{S}^{2-}$ redox couple. To prepare the Cu_2S counter electrode, two different methods are used. One is to remove Zn from the surface of brass mesh with hydrochloric acid followed by immersing the mesh in a mixed solution containing $\text{CH}_4\text{N}_2\text{S}$ and $\text{C}_2\text{H}_8\text{N}_4$ for 24 h [37]. The SEM images of resulted Cu_2S covered mesh are shown in Fig. 2a–c. The magnified SEM image indicates the granular-structured Cu_2S are formed. The cross-sectional view in Fig. 2d indicates the existence of Cu_2S film on the brass wire, the crack between them originates from cutting during the preparation of the cross-sectional sample, and the thickness is about 1.3 μm . The cross-sectional sample in Fig. 2e reveals that the only elements that exist there are Cu and S, and the atom ratio of Cu to S is approximately 2. The XPS spectra of Cu and S are shown in Fig. 2f and h, respectively. The peaks of Cu 2p at 952 eV and 932.5 eV correspond to the electron binding energy of Cu 2p_{1/2} and Cu 2p_{3/2}, respectively, which is consistent with the Cu^{1+} [38]. The peaks observed in S 2p at 163.5 eV and 161 eV

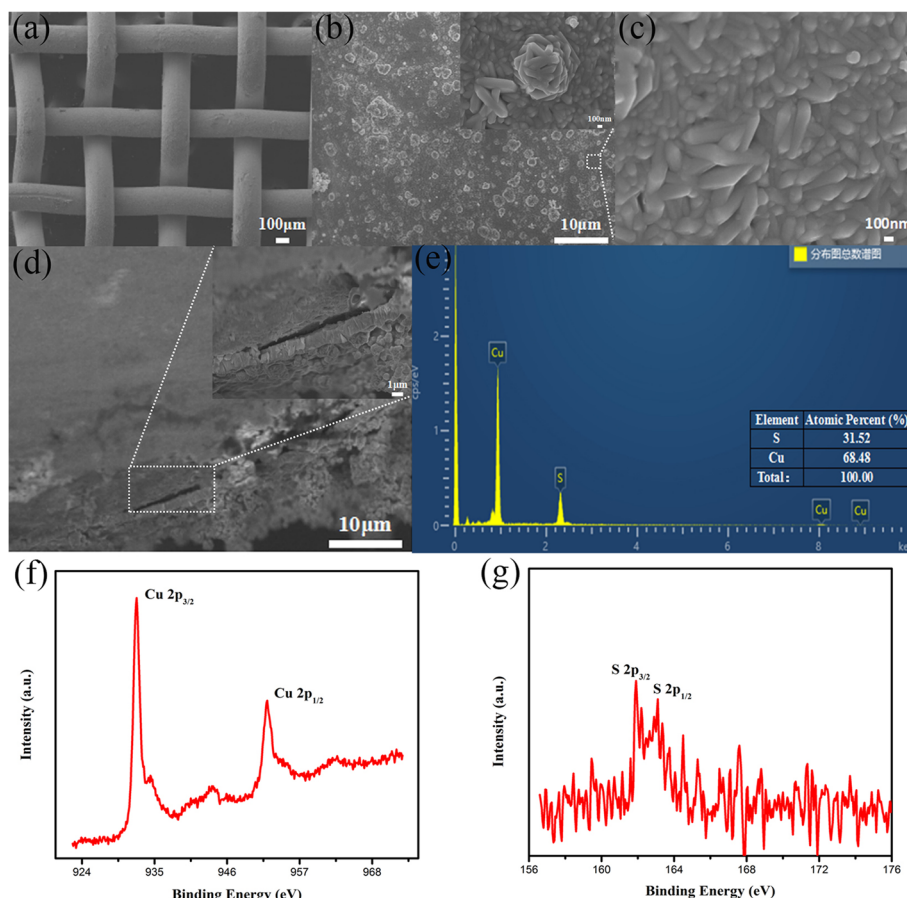


Fig. 2 SEM images of the mesh-structured Cu_2S counter electrode: **a** top view; **b, c** enlarged view of surface morphology; **d** cross-sectional view and enlarged view of the Cu_2S layer. **e** EDS of Cu_2S . **f, g** XPS survey spectrums of Cu_2S samples

correspond to S 2p_{1/2} and S 2p_{3/2}, respectively, which is consistent with S^{2−} [39]. These results confirm the successful preparation of Cu₂S film on the brass mesh, and the surface morphology is supposed to ensure its large surface area and sufficient catalytic activity.

The other method has been extensively used in previous reports, in which the brass mesh is firstly placed in hydrochloric acid, then it is subsequently dipped into the polysulfide electrolyte (1 M Na₂S and 1 M S) for a suitable time [40]. The corresponding results are shown in Fig. S2. The magnified SEM image indicates the flake-structured Cu₂S are formed. The cross-sectional view indicates the existence of Cu₂S film on the brass wire, and the thickness is also about 1.3 μm. The Cu XPS spectra show peaks at 933.1 eV and 952.5 eV, corresponding to Cu 2p_{3/2} and 2p_{1/2}, respectively [41]. The S 2p spectrum shows a peak at 162.4 eV, which confirms the presence of S^{2−} [42].

The effect of Cu₂S morphology on cell performance is further investigated.

To characterize the performance of cells with different architectures and CEs, the photocurrent density–voltage (*J*–*V*) curves are acquired and shown in Fig. 3a–d. Single photoanode device and double photoanode device are both fabricated for comparison with granular and flake Cu₂S as CEs, respectively. There are three ways for illuminating the cells: top, bottom, and double directions as shown in Fig. 4e, and the behaviors of cell working under different illumination conditions are investigated in detail, and the corresponding cell parameters are summarized in Table 1 including open-circuit voltage (*V*_{oc}), short-circuit current (*J*_{sc}), filling factor (FF), and PCE, in which the values not in brackets are the experimental average of twenty group cells and those in brackets are champion values. The test configuration for the single photoanode device with granular and flake

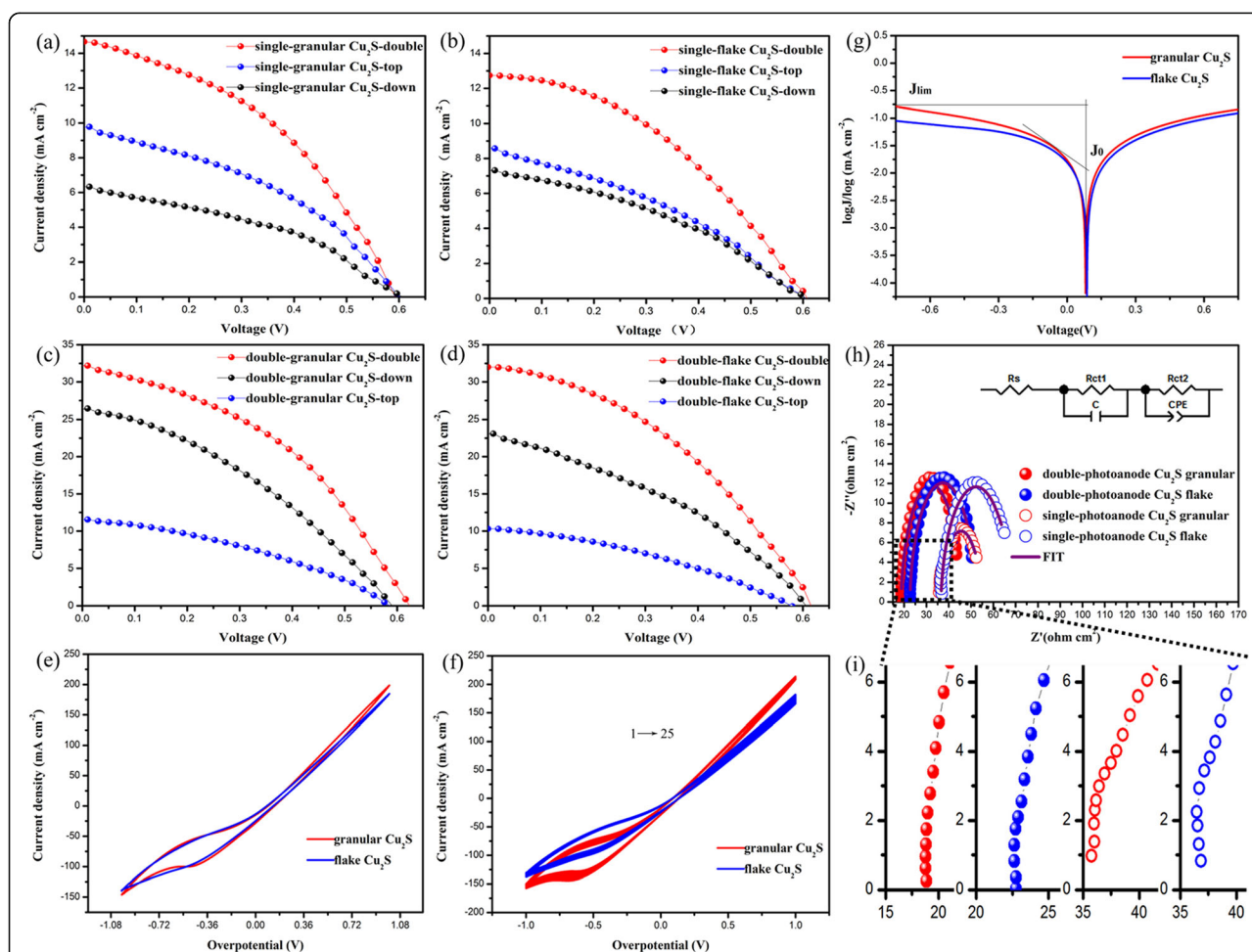


Fig. 3 Champion *J*–*V* curves of QDSSCs with different structures. **a** Single-photoanode and granular Cu₂S CE. **b** Single-photoanode and flake Cu₂S CE. **c** Double-photoanode and granular Cu₂S CE. **d** Double-photoanode and flake Cu₂S CE. **e** CV and **g** tafel polarization curves of two Cu₂S CEs, respectively. **f** Electrochemical stability of various CEs studied by CV. **h** Nyquist plots of QDSSCs with different CEs and different structures under the illumination of one full sun intensity. **i** Enlarged part of the black dotted frame in **h**

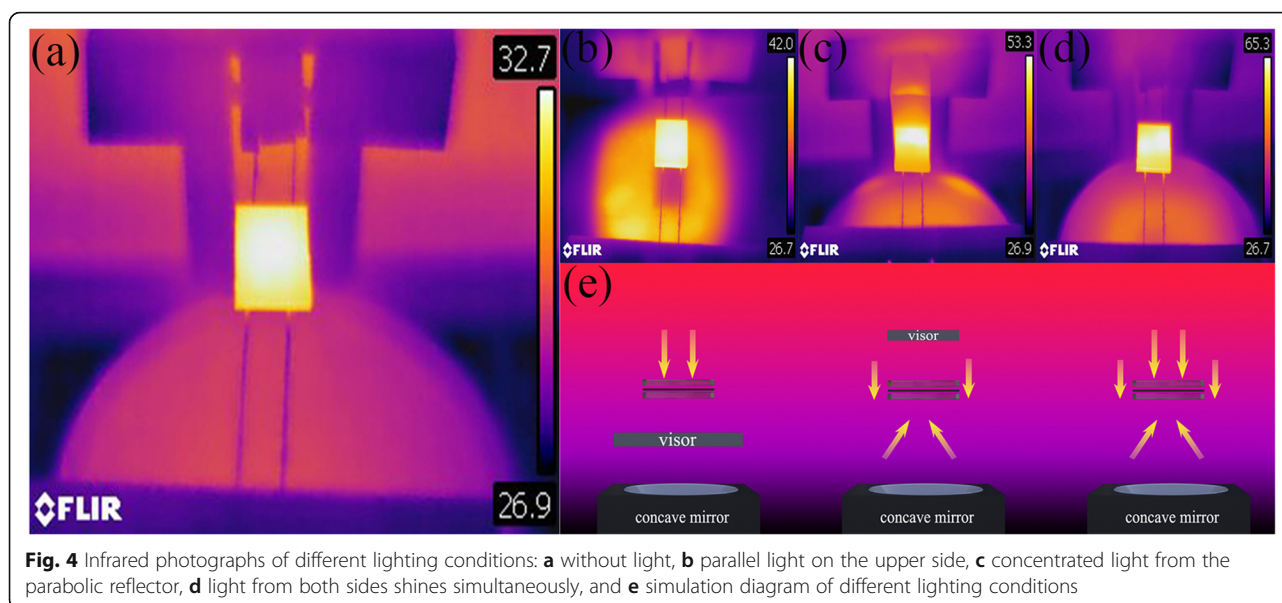


Fig. 4 Infrared photographs of different lighting conditions: **a** without light, **b** parallel light on the upper side, **c** concentrated light from the parabolic reflector, **d** light from both sides shines simultaneously, and **e** simulation diagram of different lighting conditions

Cu₂S as CEs is shown in Fig. S3, and the J - V curves are shown in Fig. 3a and b. The PCE irradiating from the top, down, and double directions are 2.32%, 2.00%, and 3.59%, respectively, while the V_{oc} are kept around 0.6 V, and the main increase in PCE is due to elevated J_{sc} . Since this is a single photoanode device, the increased J_{sc} should be due to the augmented light intensity from bottom irradiation, which results in increased photo-generated electrons in photoanodes. It should be noticed that the PCE of down irradiation is lower than that of top irradiation even if the concentrated light is higher in intensity than parallel light from the top, which could get an explanation from Fig. S3. When concentrating light on single photoanode QDSSCs, the light needs to pass through FTO glass, then through the Cu₂S mesh CE and electrolyte to reach the top photoanode,

inducing photoenergy loss to some extent. From our result, the intensity of photoenergy arriving the top photoanode would be weaker than parallel light irradiation from the top. Therefore, the PCE of the single photoanode cell structure under concentrated light irradiation is lower than that under parallel light irradiation on the upper side. It could be further supported by adopting test configuration shown in Fig. S4. Focusing light directly onto the bottom photoanode as working electrode achieves a PCE of 4.32% and a short-circuit current of 21.6 mA cm⁻², almost twice the short-circuit current generated by the parallel light irradiating the photoanode, which means that the photon flux after condensing is twice that of the parallel light from the top. From the change of photon flux, we can calculate the condensing coefficient is 2, which is consistent with our

Table 1 Parameters obtained from J - V curves of various QDSSCs under different lighting conditions. The values not in brackets are the experimental average of twenty group cells, and those in brackets are champion values

Cell	V_{oc} [V]	J_{sc} [mA cm ⁻²]	FF [%]	PCE [%]
Single-granular Cu ₂ S-top	0.583 (0.602)	9.682 (9.760)	0.394 (0.430)	2.18 (2.32)
Single-granular Cu ₂ S-down	0.599 (0.606)	6.256 (6.336)	0.407 (0.409)	1.91 (2.00)
Single-granular Cu ₂ S-double	0.584 (0.592)	14.663 (14.681)	0.402 (0.413)	3.58 (3.59)
Single-flake Cu ₂ S-top	0.604 (0.610)	8.969 (8.978)	0.381 (0.401)	1.94 (1.98)
Single-flake Cu ₂ S-down	0.594 (0.607)	7.314 (7.350)	0.401 (0.410)	1.78 (1.79)
Single-flake Cu ₂ S-double	0.590 (0.610)	13.294 (13.308)	0.378 (0.397)	2.92 (3.09)
Double-granular Cu ₂ S-top	0.573 (0.585)	11.550 (11.552)	0.391 (0.399)	2.55 (2.64)
Double-granular Cu ₂ S-down	0.582 (0.590)	26.287 (26.332)	0.353 (0.356)	5.51 (5.53)
Double-granular Cu ₂ S-double	0.616 (0.629)	32.247 (32.297)	0.395 (0.408)	8.17 (8.28)
Double-flake Cu ₂ S-top	0.561 (0.578)	10.311 (10.418)	0.356 (0.347)	2.12 (2.21)
Double-flake Cu ₂ S-down	0.586 (0.605)	22.956 (23.045)	0.336 (0.359)	4.87 (5.00)
Double-flake Cu ₂ S-double	0.616 (0.624)	32.001 (32.012)	0.396 (0.404)	7.80 (7.68)

measured results. As can be seen from Table 1, the average PCE of the double photoanode cell structure with granular Cu_2S CE is 5.51% under the condition of concentrating light from the bottom side, and the increase in PCE is due to the contribution of top photoelectrode, indicating that the top photoanode captures more photons under the concentrating condition.

For the double photoanode device with granular Cu_2S as CEs, the PCE irradiating from the top, down, and double directions are 2.64% ($J_{\text{sc}} = 11.552 \text{ mA cm}^{-2}$), 5.53% ($J_{\text{sc}} = 26.287 \text{ mA cm}^{-2}$), and 8.28% ($J_{\text{sc}} = 32.247 \text{ mA cm}^{-2}$), respectively. Compared with that of traditional single photoanode structure irradiated from the top (2.32%), the PCE increases by 260%. The increase in PCE is obviously due to the increased J_{sc} , indicating the double photoanodes work in a parallel configuration. The measured light intensity of the concentrated light from the bottom is approximately twice that of the upper parallel light. Under the irradiation condition of the concentrated light, the PCE of QDSSCs should be higher than that of the upper parallel light. It is consistent with the present result that the PCE from bottom irradiation is more than 2 times compared with that from top irradiation.

It should be noticed that the behaviors of cells based on flake Cu_2S CE are similar but showing overall decayed values in photovoltaic parameters. To explore the detailed origination, the cyclic voltammogram (CV) curves and tafel polarization curves of the two kinds of Cu_2S CEs are measured using a three-electrode system. Figure 3e is the CV curves, and granular Cu_2S shows higher current density. The reduction peak of granular Cu_2S is higher than flake Cu_2S , indicating the faster redox reaction rate of $\text{S}^{2-}/\text{S}_n^{2-}$ in the electrolyte. Figure 3f shows the CV curves of the Cu_2S electrode with different morphologies from 1 to 25 cycles. There is no obvious variation that could be found for the shape of the CV curve and the position of the peak. The CV curves overlap well under continuous scanning, indicating that the two morphologies of the electrode both own good chemical stability. It can be seen from Fig. 3g that the exchange current density (J_0) of granular Cu_2S is larger than that of flake Cu_2S . According to the test results of CV and tafel polarization curves, it suggests that the catalytic activity of granular Cu_2S is better than that of Cu_2S film. This is consistent with the photovoltaic performance of J - V curves in Fig. 3a–d. To further confirm the catalytic activity of the counter electrodes, EIS spectra are studied and shown in Fig. 3h. The purple solid lines represent fitting curves, and the fitting data are summarized in Table 2. R_{ct1} , R_{ct2} , and R_s represent charge transfer resistance on the counter electrode, charge transfer resistance at the photoanode/electrolyte interface, and series resistance, respectively. It can be

Table 2 Fitted values of R_s , R_{ct1} , and R_{ct2} of QDSSCs with different structures and morphologies from the Nyquist plots

Counter electrode	R_s (Ω)	R_{ct1} ($\Omega \text{ cm}^2$)	R_{ct2} ($\Omega \text{ cm}^2$)
Double-photoanode Cu_2S granular	18.65	5.990	20.81
Double-photoanode Cu_2S flake	22.63	8.088	21.42
Single-photoanode Cu_2S granular	35.62	3.522	15.36
Single-photoanode Cu_2S flake	36.47	6.753	25.03

seen that the structure of a single photoanode cell and the charge transfer resistances of R_{ct1} for granular Cu_2S and flake Cu_2S is 3.522 and 6.753 $\Omega \text{ cm}^2$, respectively, and those of double photoanode cell are 5.990 and 8.088 $\Omega \text{ cm}^2$, respectively. The smaller R_{ct1} of granular Cu_2S indicates better conductivity due to its smaller charge transfer resistance.

The photon flux inside an absorber conforms to Lambert–Beer law:

$$b(E, x) = [1 - R(E)]bs(E) \exp \left[- \int_0^x \alpha(E, x') dx' \right] \quad (1)$$

where $b(E, x)$ is the photon flux received by QDs at position x , $bs(E)$ is the photon flux received in the vertical direction to solar irradiation, $R(E)$ is the reflectivity of the interface, and $\alpha(E, x)$ is the absorption coefficient at position x . CPV collect incident light over a large area and focus it on a small area of solar cell for photovoltaic conversion. Concentration factor X is an important parameter to describe the performance of concentrating solar cells, which is the increased times of photon flux density $b(E)$ and is also approximated to be the ratio of the area of collected incident light to the area of solar cells. It could be considered that the focused light is uniform within the half angle of concentration (θ_x), and the increased times of solar photon flux $b_s(E, x)$ equals to concentration factor X . Therefore, for CPV, Eq. (1) could be expressed as:

$$b(E, x) = [1 - R(E)] \cdot X \cdot bs(E) \exp \left[- \int_0^x \alpha(E, x') dx' \right] \quad (2)$$

The photocurrent (J_{ph}) generated by a solar cell under light conditions, determined by the photon flux and the performance of the solar cell, J_{ph} is equal to J_{sc} , and can be expressed as:

$$J_{\text{ph}} = J_{\text{sc}} = q \int_0^\infty QE(E)bs(E, Ts)dE \quad (3)$$

where Q is the elementary charge. quantum efficiency (QE) is a function of photon energy. We assume that the photon flux of the collector bs_2 is Y times that of the top

photon flux bs_1 , and the J_{sc} of the double photoanode cell under irradiation from the down side could be expressed as:

$$J_{sc}(Ybs) = q \int_0^{\infty} QE(E) \cdot Y \cdot bs(E, Ts) dE \approx YJ_{sc} \quad (4)$$

Therefore, the sum of J_{sc1} value under the condition of parallel light irradiation from the top side and J_{sc2} value under the condition of concentrated light irradiation from the down side should be equal to $J_{sc1, 2}$ generated by light irradiation on both sides of the PV. Equation (4) is basically consistent with J - V results in Table 1, however with some deviations. As can be seen from the J_{sc} data, the sum of J_{sc1} illuminating from the top and J_{sc2} illuminating from the down is a little smaller than that of $J_{sc1, 2}$ illuminating from both sides for double photoanode devices. The deviation should result from the photothermal effect due to the temperature variation of QDSSCs under different illuminating conditions.

It is well known that the focused light on optoelectrical devices would induce thermal accumulation and increased temperature. In the present work, the photon flux of the concentrated light from the parabolic reflector measured by the light intensity meter is approximately twice the normal sunlight simulator; it means that the concentration coefficient is 2, which is much smaller than practical CPV devices. However, it is still necessary to investigate the effect of thermal accumulation on the cell. We use an infrared (IR) camera to monitor the temperature variation under different testing conditions. The focal length of the used parabolic reflector is 6.5 cm. We place the photovoltaic device 0.5 cm below the focus point of the parabolic reflector to ensure the full illumination of the active area, which is about 1.5 cm^2 . The IR temperature images for double photoanode devices are shown in Fig. 4b–d, and the corresponding irradiation conditions are shown in Fig. 4e. Compared with non-irradiated devices, the temperature increases are 9.3°C , 20.6°C , and 32.6°C , respectively. The double side irradiation shows a higher temperature increase than the sum of separate irradiation from the top and down, which indicates the additional mechanism from the material or interface involved here. The reaction of S^{2-}/S_n^{2-} in electrolyte and interface is not similar under different temperatures. According to the Arrhenius formula, the chemical reaction rate in PV increases with the increase of temperature. With the increase of temperature, the redox reaction near the QDSSC electrodes was enhanced, which accelerated the depletion of photogenic holes in the photoanode, thus greatly reducing the energy-excited redox reaction.

Conclusions

In summary, we design a new solar cell architecture by integrating the CPV concept into QDSSCs with double photoanode design. To ensure the better light harvesting, the Cu_2S mesh is used as a counter electrode and sandwiched between two photoanodes, and the effect of Cu_2S morphology on cell performance is investigated and optimized. It has been shown that the special design achieved a 260% enhancement in PCE compared with the single photoanode irradiated from the top side. While the open voltage circuit does not change, the double photoanode design greatly increases the current density and thus increases PCE. In addition, the photothermal effect induced by CPV could be helpful to improve PCE, and a champion PCE of 8.28% ($V_{oc} = 0.629 \text{ V}$, $J_{sc} = 32.247 \text{ mA cm}^{-2}$) is achieved. It should be mentioned that the present does provide a new way for boosting PCE of QDSSCs, but the device design specially for the CPV part could be further optimized, and the performance of the cell would be further enhanced. We believe that with better QD sensitizers and device design techniques, the idea suggested in the present work would induce great progress in QDSSCs and could be expanded to other solar cells.

Supplementary information

Supplementary information accompanies this paper at <https://doi.org/10.1186/s11671-020-03424-8>.

Additional file 1: Figure S1. The cross-section SEM of TiO_2 photoanode. **Figure S2.** SEM top view (a) and cross-sectional view (b) of flake Cu_2S ; (c) and (d) are XPS spectra of Cu and S. The XPS spectra of as-prepared flake Cu_2S CEs show peaks at 933.1 eV and 952.5 eV, corresponding to Cu 2p_{3/2} and 2p_{1/2}, respectively. The S 2p spectrum shows a peak at 162.4 eV, which confirms the presence of S^{2-} . **Figure S3.** Schematic illustration of a single-photoanode structure for J-V measurement irradiated from downside. It needs to penetrate the bottom photoanode, electrolyte and Cu_2S mesh structure to arrive the top photoanode. **Figure S4.** When the light is condensed by a parabolic reflector and irradiates from the bottom photoanode, it can generate a short circuit current of about 21.6 mA cm^{-2} , almost twice the short-circuit current generated by the parallel light irradiating the photoanode, which means that the photon flux after condensing is twice that of the parallel light from top. From the change of photon flux, we can calculate the condensing coefficient is 2, which is consistent with our measured results. **Figure S5.** The PCE of cells using the Cu_2S mesh CE composed of 0.22 mm copper wires was 6.79% and 6.25%, respectively. The diameter of the Cu wire is inversely related to the aperture of the Cu mesh. In this work, the diameter of the Cu mesh used is 0.25 mm. The PCE results for a Cu mesh CE with wire diameter of 0.22 mm are shown in Figure S5, which are lower than that of 0.25 mm Cu mesh.

Abbreviations

QDSSCs: Quantum dot-sensitized solar cells; PCE: Power conversion efficiency; CPV: Concentrating solar cell; QDs: Quantum dots; FF: Fill factor; SILAR: Successive ionic layer adsorption and reaction; CV: Cyclic voltammetry; CBD: Chemical bath deposition; SEM: Scanning electron microscopy; XPS: X-ray photoelectron spectra

Authors' Contributions

RR and WL conceived the idea. PX carried out the experiments. XP and PX participated in the preparation of the samples. LY, XJ, XS, DJ, and XY took

part in the experiments and the discussion of the results. RR and WL drafted the manuscript. The authors read and approved the final manuscript.

Funding

This work was financially supported by the National Natural Science Foundation of China (Grant No. 61574021), the Natural Science Foundation of Jilin Province (Grant No. 20190201105JC), the Science Foundation of Jilin Education Department (Grant No. JJKH20200661KJ, JJKH20191288KJ), and Capital construction funds within the provincial budget (Grant No. 2019C046-8).

Availability of Data and Materials

The datasets used or analyzed during the current study are available from the corresponding author on reasonable request.

Competing Interests

The authors declare that they have no competing interests.

Received: 9 August 2020 Accepted: 22 September 2020

Published online: 29 September 2020

References

- Elibol E (2020) Effects of different counter electrodes on performance of CdSeTe alloy QDSSC. *Sol Energy* 197:519–526
- Huang F, Hou J, Zhang Q, Wang Y, Massé RC et al (2016) Doubling the power conversion efficiency in CdS/CdSe quantum dot sensitized solar cells with a ZnSe passivation layer. *Nano Energy* 26:114–122
- Sun J-K, Jiang Y, Zhong X, Hu J-S, Wan L-J (2017) Three-dimensional nanostructured electrodes for efficient quantum-dot-sensitized solar cells. *Nano Energy* 32:130–156
- Seol M, Youn DH, Kim JY, Jang JW, Choi M et al (2014) Mo-compound/CNT-graphene composites as efficient catalytic electrodes for quantum-dot-sensitized solar cells. *Adv Energy Mater* 4:1300775
- Wang M, Zai J, Li B, Wang Y, Huang S et al (2016) Hierarchical Cu₂xSe nanotubes constructed by two-unit-cell-thick nanosheets: room-temperature synthesis and promoted electrocatalytic activity towards polysulfides. *J Mater Chem A* 4:4790–4796
- Halder G, Bhattacharyya S (2017) Zinc-diffused silver indium selenide quantum dot sensitized solar cells with enhanced photoconversion efficiency. *J Mater Chem A* 5:11746–11755
- Huang H, Pan L, Lim CK, Gong H, Guo J et al (2013) Hydrothermal growth of TiO₂ nanorod arrays and in situ conversion to nanotube arrays for highly efficient quantum dot-sensitized solar cells. *Small* 9:3153–3160
- Kriegel I, Jiang C, Rodríguez-Fernández J, Schaller RD, Talapin DV et al (2012) Tuning the excitonic and plasmonic properties of copper chalcogenide nanocrystals. *J Am Chem Soc* 134:1583–1590
- Li Y, Pan G, Liu Q, Ma L, Xie Y et al (2018) Coupling resonances of surface plasmon in gold nanorod/copper chalcogenide core-shell nanostructures and their enhanced photothermal effect. *ChemPhysChem* 19:1852–1858
- Zheng L, Teng F, Ye X, Zheng H, Fang X (2020) Photo/electrochemical applications of metal sulfide/TiO₂ heterostructures. *Adv Energy Mater* 10:1902355
- Du J, Du Z, Hu J-S, Pan Z, Shen Q et al (2016) Zn-Cu-In-Se quantum dot solar cells with a certified power conversion efficiency of 11.6%. *J Am Chem Soc* 138:4201–4209
- Wang W, Feng W, Du J, Xue W, Zhang L et al (2018) Cosensitized quantum dot solar cells with conversion efficiency over 12%. *Adv Mater* 30:1705746
- Pan Z, Yue L, Rao H, Zhang J, Zhong X et al (2019) Boosting the performance of environmentally friendly quantum dot-sensitized solar cells over 13% efficiency by dual sensitizers with cascade energy structure. *Adv Mater* 31:1903696
- Zhang H, Ji X, Liu N, Zhao Q (2019) Synergy effect of carbon nanotube and graphene hydrogel on highly efficient quantum dot sensitized solar cells. *Electrochim Acta* 327:134937
- Jose R, Thavasi V, Ramakrishna S (2009) Metal oxides for dye-sensitized solar cells. *J Am Chem Soc* 92:289–301
- Wang X, Koleilat GI, Tang J, Liu H, Kramer IJ et al (2011) Tandem colloidal quantum dot solar cells employing a graded recombination layer. *Nat Photonics* 5:480–484
- Choi JJ, Wenger WN, Hoffman RS, Lim YF, Luria J et al (2011) Solution-processed nanocrystal quantum dot tandem solar cells. *Adv Mater* 23:3144–3148
- Sahasrabudhe A, Kapri S, Bhattacharyya S (2016) Graphitic porous carbon derived from human hair as 'green' counter electrode in quantum dot sensitized solar cells. *Carbon* 107:395–404
- Li L, Hao Y, Yang X, Zhao J, Tian H et al (2011) A double-band tandem organic dye-sensitized solar cell with an efficiency of 11.5%. *Chem Sus Chem* 4:609–612
- Yamaguchi T, Uchida Y, Agatsuma S, Arakawa H (2009) Series-connected tandem dye-sensitized solar cell for improving efficiency to more than 10%. *Sol Energy Mater Sol Cells* 93:733–736
- Yanagida M, Onozawa-Komatsuzaki N, Kurashige M, Sayama K, Sugihara H (2010) Optimization of tandem-structured dye-sensitized solar cell. *Sol Energy Mater Sol Cells* 94:297–302
- Yang Y-Y, Zhang Q-X, Wang T-Z, Zhu L-F, Huang X-M et al (2013) Novel tandem structure employing mesh-structured Cu₂S counter electrode for enhanced performance of quantum dot-sensitized solar cells. *Electrochim Acta* 88:44–50
- Wang F, Wang H, Liu X, Wu D, Jiang K et al (2018) Full-spectrum liquid-junction quantum dot-sensitized solar cells by integrating surface plasmon-enhanced electrocatalysis. *Adv Energy Mater* 8:1800136
- Kil T-H, Kim S, Jeong D-H, Geum D-M, Lee S et al (2017) A highly-efficient, concentrating-photovoltaic/thermoelectric hybrid generator. *Nano Energy* 37:242–247
- Litvin A, Martynenko I, Purcell-Milton F, Baranov A, Fedorov A et al (2017) Colloidal quantum dots for optoelectronics. *J Mater Chem A* 5:13252–13275
- Daenke T, Uemura Y, Duffy NW, Mozer AJ, Koumura N et al (2012) Aqueous dye-sensitized solar cell electrolytes based on the ferricyanide-ferrocyanide redox couple. *Adv Mater* 24:1222–1225
- Esfandarypour M, Garnett EC, Cui Y, McGehee MD, Brongersma ML (2014) Metamaterial mirrors in optoelectronic devices. *Nat Nanotechnol* 9:542–547
- Haque S, Mendes MJ, Sanchez-Sobrado O, Águas H, Fortunato E et al (2019) Photonic-structured TiO₂ for high-efficiency, flexible and stable perovskite solar cells. *Nano Energy* 59:91–101
- Zhang Z, Wang Y, Hansen PAS, Du K, Gustavsen KR et al (2019) Black silicon with order-disordered structures for enhanced light trapping and photothermal conversion. *Nano Energy* 65:103992
- Qiao F, Xie Y, He G, Chu H, Liu W, et al. Light trapping structures and plasmons synergistically enhance the photovoltaic performance of full-spectrum solar cells. *Nanoscale*. 2020;12:1269–80.
- Cavalli A, Dijkstra A, Haverkort JE, Bakkers EP (2018) Nanowire polymer transfer for enhanced solar cell performance and lower cost. *Nano-Structures Nano-Objects* 16:59–62
- Apostoleris H, Stefancich M, Chiesa M (2016) Tracking-integrated systems for concentrating photovoltaics. *Nat Energy* 1:1–8
- Philipps SP, Bett AW, Horowitz K, Kurtz S. Current status of concentrator photovoltaic (CPV) technology. 2015. TP-5J00-65130.
- Han C, Bai Y, Sun Q, Zhang S, Li Z et al (2016) Ambient aqueous growth of Cu₂Te nanostructures with excellent electrocatalytic activity toward sulfide redox shuttles. *Adv Sci* 3:1500350
- Meng X, Yu C, Song X, James L et al (2018) Scrutinizing defects and defect density of selenium-doped graphene for high-efficiency triiodide reduction in dye-sensitized solar cells. *Angew Chem Int Ed* 17:4682–4686
- Meng X, Yu C, Zhang X, Huang L (2018) Active sites-enriched carbon matrix enables efficient triiodide reduction in dye-sensitized solar cells: an understanding of the active centers. *Nano Energy* 54:138–147
- Wang L, Ji R, Yu L, Wang G, Zhang X (2013) Study on the electrochemical oxidation of glucose on different Cu-Cu₂S integrated electrodes. *Anal Methods* 5:4476–4479
- Mínguez-Bacho I, Courté M, Shi C, Fichou D (2015) Controlling the nanomorphology of thin conformal Cu₂S overlayers grown on Cu₂O compact layers and nanowires. *Mater Lett* 159:47–50
- Hossain MA, Jennings JR, Shen C, Pan JH, Koh ZY et al (2012) CdSe-sensitized mesoscopic TiO₂ solar cells exhibiting >5% efficiency: redundancy of CdS buffer layer. *J Mater Chem* 22:16235–16242
- Shi C, Dong H, Zhu R, Li H, Sun Y et al (2015) An "all-in-one" mesh-typed integrated energy unit for both photoelectric conversion and energy storage in uniform electrochemical system. *Nano Energy* 13:670–678
- Selopal GS, Chahine R, Mohammadnezhad M, Navarro-Pardo F, Benetti D et al (2019) Highly efficient and stable spray assisted nanostructured Cu₂S/

carbon paper counter electrode for quantum dots sensitized solar cells. *J Power Sources* 436:226849

42. Ye M, Chen C, Zhang N, Wen X, Guo W et al (2014) Quantum-dot sensitized solar cells employing hierarchical Cu₂S microspheres wrapped by reduced graphene oxide nanosheets as effective counter electrodes. *Adv Energy Mater* 4:1301564

Publisher's Note

Springer Nature remains neutral with regard to jurisdictional claims in published maps and institutional affiliations.

Submit your manuscript to a SpringerOpen[®] journal and benefit from:

- Convenient online submission
- Rigorous peer review
- Open access: articles freely available online
- High visibility within the field
- Retaining the copyright to your article

Submit your next manuscript at ► [springeropen.com](https://www.springeropen.com)